Journal of Colloid and Interface Science **248,** 389–397 (2002)
doi:10.1006/jcis.2002.8241, available online at http://www.idealibrary.com on IDEAL®

Hamaker Constants in Integrated Circuit Metalization

Sean Eichenlaub,* Carly Chan,*,† and Stephen P. Beaudoin*,[1]

*Department of Chemical and Materials Engineering, Arizona State University, Tempe, Arizona 85287; and †Department of Chemical Engineering, University of Michigan, Ann Arbor, Michigan 48109

Received August 31, 2001; accepted January 14, 2002; published online March 13, 2002

A new method for determining Hamaker constants was examined for materials of interest in integrated circuit manufacture. An ultra-high vacuum atomic force microscope and an atomic force microscope operated in a nitrogen environment were used to measure the interaction forces between metals, dielectrics, and barriers used during the metalization portion of integrated circuit manufacturing. The materials studied included copper, silver, titanium nitride, silicon dioxide, poly(tetrafluoroethylene), and parylene-N. Spheres coated with a material of interest were mounted on AFM cantilevers and brought into contact with substrates of interest. The interaction force was measured as the cantilever approached the substrate but before the two surfaces came into contact, and also when the particle was pulled out of contact with the substrate. The Hamaker constant calculation from the contact measurement is based on an adhesion model that quantifies the contribution of geometrical, morphological and mechanical properties of materials to the measured adhesion force. Hamaker constants determined with this new approach were compared with values found by using the Derjaguin approximation for a sphere to describe the interaction force as the cantilever approaches the surface. Both approaches produced similar values for most of the systems studied, with variations of less than 10%. © 2002 Elsevier Science (USA)

Key Words: **Hamaker constants; van der Waals forces; adhesion; electronic thin films; atomic force microscopy.**

INTRODUCTION

As new thin film materials are introduced into integrated circuits (ICs), the adhesion between these films and the adhesion of fine particles to these films must be understood. Of particular interest are metals such as copper and silver (1–3) and dielectric polymers such as parylene, polyimide, and vapor deposited poly(tetrafluoroethylene) (PTFE) (3–5). Proper understanding of the adhesion between these materials is required to ensure films remain adhered and particle contamination is minimized, and also to guide the rational selection of new materials.

van der Waals (VDW) forces are one of several forces that control the adhesion between two materials. VDW forces are important to quantify in adhesion studies because they are always present and are always attractive. VDW forces dominate the interaction of particles in contact with thin films (6–9) and can also be the controlling forces in film adhesion, contributing to adhesive or cohesive film failure (9). Within the equation that describes VDW forces, the Hamaker constant is a key parameter that describes how strongly two materials interact. The range of literature Hamaker constant values for a given system can be considerable. Additionally, literature values cannot be found for many new systems. In this paper, a new approach for determining Hamaker constants is described and demonstrated for metals, barriers, and dielectrics of interest to the IC industry. Hamaker constants were determined experimentally with an ultra-high vacuum (UHV) atomic force microscope (UHVAFM), and with an AFM in a nitrogen ambient. Spheres covered with surface films of interest were mounted on AFM cantilevers and brought into and out of contact with substrates of interest. The interaction force was recorded as a function of the particle/substrate separation distance. The Hamaker constants were determined using two methods. First, the Derjaguin approximation was used to describe the observed interaction force as the spheres on the AFM cantilever approached the substrates. A number of authors have used this approach (10–12). This method was pursued as a basis of comparison with a new method developed here. The new method involved bringing the spheres into contact with the surface and measuring the interaction force as they are pulled out of contact. The Hamaker constant is calculated from the force measured as the cantilever is removed from the surface using an adhesion model developed previously (6–9) which accounts for the effects of surface roughness, particle geometry, and elastic properties of the interacting materials in the measured adhesion force. In this work Hamaker constants were determined for interactions involving copper, silver, titanium nitride, silicon dioxide, parylene-N, and PTFE. The experimentally measured values for the Hamaker constants were compared with literature values, as well as with Hamaker constants calculated from literature values of the spectral and optical properties of these materials.

THEORY

Steric forces, electrostatic forces, hydrogen bonding, chemical bonding, capillary forces, and dispersion forces (or VDW forces) may be present in all particle/thin film or thin film/thin

[1] To whom correspondence should be addressed. E-mail: steve.beaudoin@asu.edu.

0021-9797/02 $35.00
© 2002 Elsevier Science (USA)
All rights reserved.

film systems. While the forces present in any given system are dictated by the nature of the system of interest, VDW forces are always present. VDW forces have three components: Debye forces or permanent dipole-permanent dipole interactions, Keesom forces or permanent dipole-induced dipole interactions, and London dispersion forces or induced dipole-induced dipole interactions (13, 14).

The Hamaker constant, the force law scaling constant of the VDW force, can be calculated from spectral or optical properties of materials. There are several ways to calculate the Hamaker constant based on this information, including the full spectral method developed by Lifshitz (15, 16), and several approximations to this method, including the simple spectral (SS) method (17–20), the Tabor Winterton (TWA) approximation (21), and the single oscillator approximation (22).

To calculate the Hamaker constant using the full spectral method (13, 15, 16, 22, 23), complex optical properties of the materials involved are required. One of these is the dependence of the dielectric properties of a material on the frequency of incident electromagnetic radiation, which takes into account how one material responds to the electromagnetic field generated by a neighboring material. The complex frequency-dependent dielectric response function, $\varepsilon(\omega)$, is represented by

$$\varepsilon(\omega) = \varepsilon'(\omega) + \varepsilon''(\omega) \quad [1]$$

where ε' and ε'' correspond to the absorption and transmission of radiation of frequency ω by the material. The Kramers–Kronig relation (18) gives the relationship between the real and imaginary parts of any optical property and is the integral transform of the imaginary part of the dielectric constant (ε, the dielectric response function) from a function of the real frequency, ω, to a function of the imaginary frequency, ξ, and is defined by

$$\varepsilon(\xi) = 1 + \frac{2}{\pi}\int_0^\infty \frac{\omega\varepsilon(\omega)}{\omega^2+\xi^2}\,d\omega. \quad [2]$$

The Hamaker constant is given by

$$A_{123} = \frac{3kT}{2}\sum_{n=0}^{\infty}{}'\sum_{s=1}^{\infty}\frac{(\Delta_{32}\Delta_{12})^s}{s^2}, \quad [3]$$

where k is Boltzmann' s constant, s and n are multiple indices of the frequency of the incident radiation, and T is the system temperature. A_{123} is the Hamaker constant for surface 1 interacting with surface 3 through medium 2. Δ_{32} and Δ_{12} are the differences in the dielectric response of the three materials and are given by

$$\Delta_{ij} = \frac{\varepsilon_i(\xi) - \varepsilon_j(\xi)}{\varepsilon_i(\xi) + \varepsilon_j(\xi)} \quad [4]$$

and

$$\xi = \left(\frac{4\pi^2 kT}{h}\right)n, \quad [5]$$

where ε_j is the dielectric response function of a given material at wavelength j and n is an integer from Eq. [3]. The major difficulty and most of the work associated with full spectral determination of Hamaker constants is involved in determining $\varepsilon_i(\xi)$. Several approximations deal with this difficulty and can be used when there is limited dielectric data available. In the SS method (17–20), the dielectric response function, $\varepsilon(i\xi)$, is represented by a model based on a damped oscillator. For many dielectrics it is assumed that

$$\varepsilon(i\xi) = 1 + \frac{C_{IR}}{1+\left(\frac{\xi}{\omega_{IR}}\right)^2} + \frac{C_{UV}}{1+\left(\frac{\xi}{\omega_{UV}}\right)^2}, \quad [6]$$

where C_{IR} and C_{UV} are the absorption strengths in the IR and UV range and ω_{IR} and ω_{UV} represent the characteristic absorption frequencies in the IR and UV range. C_{IR} and C_{UV} are parameters used to fit physical property data such as ξ and $\varepsilon(i\xi)$. C_{UV} and ω_{UV} can also be determined from Cauchy plots of refractive index and frequency. C_{IR} is then estimated by

$$C_{IR} = \varepsilon_o - C_{UV} - 1. \quad [7]$$

The TWA method uses indices of refraction to approximate the dielectric response of a material (13, 21, 22). The TWA method determines Hamaker constants as

$$A_{123} = \frac{3\pi\hbar\nu_e}{4\sqrt{2}}\frac{\left[\left(n^2_{vis0,1} - n^2_{vis0,2}\right)\left(n^2_{vis0,3} - n^2_{vis0,2}\right)\right]}{\left[\left(n^2_{vis0,1} + n^2_{vis0,2}\right)^{1/2}\left(n^2_{vis0,3} + n^2_{vis0,2}\right)^{1/2}\left(\left(n^2_{vis0,1} + n^2_{vis0,2}\right)^{1/2} + \left(n^2_{vis0,3} + n^2_{vis0,2}\right)^{1/2}\right)\right]}, \quad [8]$$

where $n_{visi,j}$ is the index of refraction for energy in the visible range. The $vis0$, j notation describes the limiting index for refraction in the visible range of material j. The characteristic absorption frequency, ν_e, is assumed to be equivalent for all three materials. It is typically accepted that Hamaker constants can be measured or predicted accurately to within 10% using these techniques. In this paper the Hamaker constants were calculated using optical properties found in the literature in the SS and TWA approximations as a basis for comparison with the experimentally measured values.

The Hamaker constant was experimentally determined in two ways. Both methods used an AFM to measure the VDW forces between substrates of interest and spheres coated with materials of interest. Both approaches for determining the Hamaker constant were performed in nitrogen gas and in UHV (1×10^{-9} Torr). A standard method was used where the VDW forces were measured as the spheres approached the surface,

but before they came into contact. The Hamaker constant was found in these studies by fitting the Derjaguin approximation for van der Waals forces between a sphere and a flat plane to the measured interaction force as the cantilever approached the surface

$$F = -\frac{A_{123}}{6h^2} R_1, \quad [9]$$

where h is the sphere–substrate separation distance and R_1 is the radius of the sphere. The forces were measured at small separation distances, less than 30∼35 nm. At these separations, VDW forces were assumed to be the dominant interaction forces and electrostatic forces were ignored (12).

The adhesion forces were also measured by bringing the spheres into contact with the surface and measuring the force required to pull them off. An adhesion model described elsewhere was used to interpret these pull-off measurements (6–8). This model isolates the contribution of the geometry, morphology, and mechanical properties of the two surfaces to the adhesion force, so that the VDW forces between the surfaces can be described and the Hamaker constant can be determined. There are three parameters that are characterized and used as inputs into the adhesion model; the roughness of both interacting surfaces, the contact area between the two surfaces, and the bulk modulus of the materials. An AFM is used to scan the surfaces of the materials in order to measure the surface roughness. Three parameters are used to describe surface roughness; the average asperity height, the standard deviation about the average asperity height, and the fractional coverage of the surface by asperities. Asperities in this work are modeled as hemispheres. The particle shape, the particle–substrate contact area, and the particle and substrate roughness are used to generate two mathematical model surfaces representative of the interacting surfaces. The material with the lower bulk modulus is assumed to deform in contact, and the bulk modulus of the more deformable material is used to calculate the compression and deformation of the surface asperities based on the VDW forces and any applied load. The VDW forces are summed over discretized elements in both surfaces to find the total VDW interaction between the two model surfaces. The discretized elements are cylinders of equal diameter. The model describes the interaction force between two opposing cylindrical volume elements in each surface

$$F = \frac{A_{123}}{6\pi} \frac{1}{h^3} A_{area}, \quad [10]$$

where h is the separation distance between the two surface elements, and A_{area} is the surface area of each the interacting elements.

This model has been validated through measurements of the interaction forces between polystyrene latex (PSL) spheres and silicon dioxide substrates in aqueous solution (6–9). The model has also been validated for asymmetrical alumina particles interacting with substrates of silicon dioxide and copper in both water and air (7–9).

Previously, this model has been used with Hamaker constants from the literature to predict adhesion forces in various systems (9). If the removal force and model parameters are measured, then this model can be used to predict the system Hamaker constant.

EXPERIMENTAL METHODS

The materials studied include parylene-N, crosslinked parylene-N, silicon dioxide, copper, silver, titanium nitride, and PTFE. The parylene substrates were obtained from Paratek and consisted of a 6000 Å layer of parylene on a silicon substrate. The silver and titanium nitrate substrates were deposited in the cleanroom of the Center for Solid State Electronics Research (CSSER) at ASU by DC magnetron sputtering and were 10,000 and 15,000 Å thick, respectively. The silicon dioxide substrates were obtained from Silica Tek. The copper substrates were sputter-deposited films purchased from Thin Film Concepts. These films were 300 Å thick. The PTFE substrates were provided by researchers at MIT and were prepared with a new deposition process (5). These films were between 6,000 and 10,000 Å thick.

PSL spheres with or without surface thin film coatings were mounted on tipless AFM cantilevers using a method developed by Ducker *et al.* and Cooper *et al.* (7, 8, 25). The polystyrene spheres had an average diameter of 5 μm and were purchased from Duke Scientific. Copper wires, etched to a point in a nitric acid solution, were used with micromanipulators to apply a layer of Norland Optical Adhesive 860 to the end of the cantilever and to pick up a sphere and deposit it on the glue on the cantilever. The cantilever was then exposed to UV light to cure the glue. The light was oriented at various angles to ensure complete curing. Figure 1 depicts a representative particle mounted on the end of the cantilever.

The PSL spheres were coated with silver, copper, and silicon dioxide. The coatings were applied before the spheres were mounted on the cantilevers. The deposited layers of silver and copper were approximately 9000 Å thick. These materials were deposited using a Torrvac evaporator in the CSSER cleanroom. The deposited layers of silicon dioxide were 2000 Å thick and were deposited using an MRC sputter apparatus. These deposited layers were of a thickness large enough that the underlying material did not affect the adhesion measurements (6). An AFM scan of the surface of a silver thin film on an AFM cantilever is shown in Fig. 2.

The spring constants of the cantilevers were determined using the method developed by Cleveland *et al.* (26). In this method the change in resonant frequency of the cantilever is measured after a mass has been applied to the end of the cantilever. The mass is determined from SEM micrographs and the density of the end mass material. The resonant frequency was determined by operating the AFM in noncontact mode.

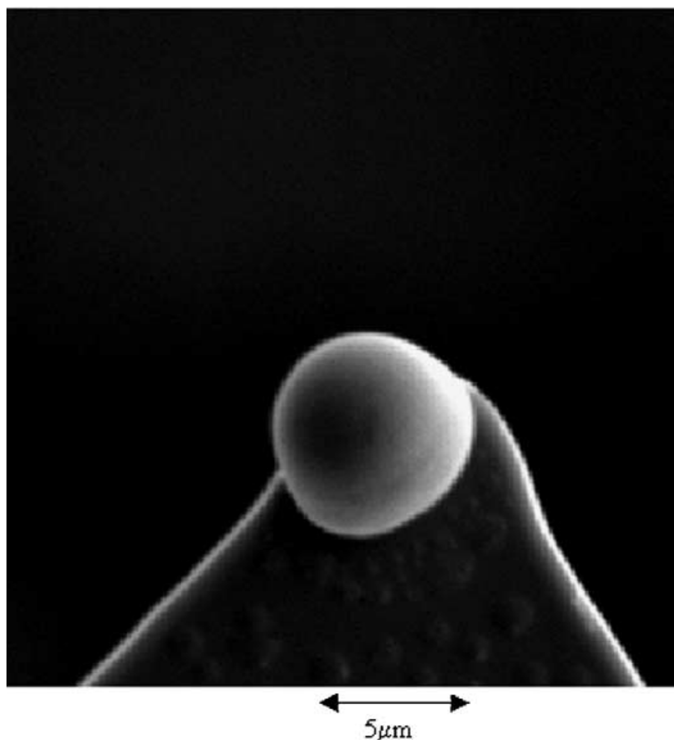

FIG. 1. SEM micrograph of a silver-coated 5 μm PSL sphere mounted on the end of an AFM cantilever.

Models described by Cooper *et al*. (6–8) allow the effects of surface roughness, particle geometry, and material mechanical properties to be isolated from a measured adhesion force between a particle and a surface. This isolates the intrinsic adhesion between the two materials. As mentioned above, the surface roughness, the bulk modulus, and the shape of the particle are required in order to use this model. The surface roughness of the spheres and substrates was measured using a Molecular Imaging AFM. The bulk modulus was measured using a Digital Instruments AFM combined with a Hysitron Inc. nanoindentor and software (27). Finally, a JSM-840 SEM was used to take SEM micrographs of the spheres on the AFM cantilevers. These were then used to measure the radius of the coated spheres.

Force measurements were made with two AFMs. All measurements made in a gaseous nitrogen ambient were made using a Molecular Imaging AFM with an environmental chamber. A dry nitrogen gas line was attached to the chamber and desiccant was kept in the bottom of the chamber in order to control the humidity. Humidity was held at less than 10%, which was beyond the sensitivity of our detector. The role of humidity in force measurements has been well established and low values are required in order to eliminate a capillary effect due to adsorbed moisture (28, 29). The samples were placed on a controlled temperature stage and were heated to 115°C for 5 min in order to drive off as much adsorbed water as possible. The samples were then allowed to cool in the nitrogen environment before measuring the interaction force between the mounted cantilever and the surface. All measurements made in ultra high vacuum were made with a Park Scientific Instruments AutoProbe VP AFM (the UHVAFM). As in the nitrogen environment, samples were heated to 115°C for 5 min in the UHVAFM before measuring the interaction force between the cantilever and the sample surface. The UHVAFM measurements were made at 1–2 $\times$ 10^{-10} Torr. The vertical scan rate of the AFM was set at 2 Hz or less during the measurements in nitrogen and at UHV. At this scan rate the sphere on the cantilever is in contact with the surface for less than 0.5 s, which is less time than is required to reach full plastic deformation under a small applied load (7, 30, 31).

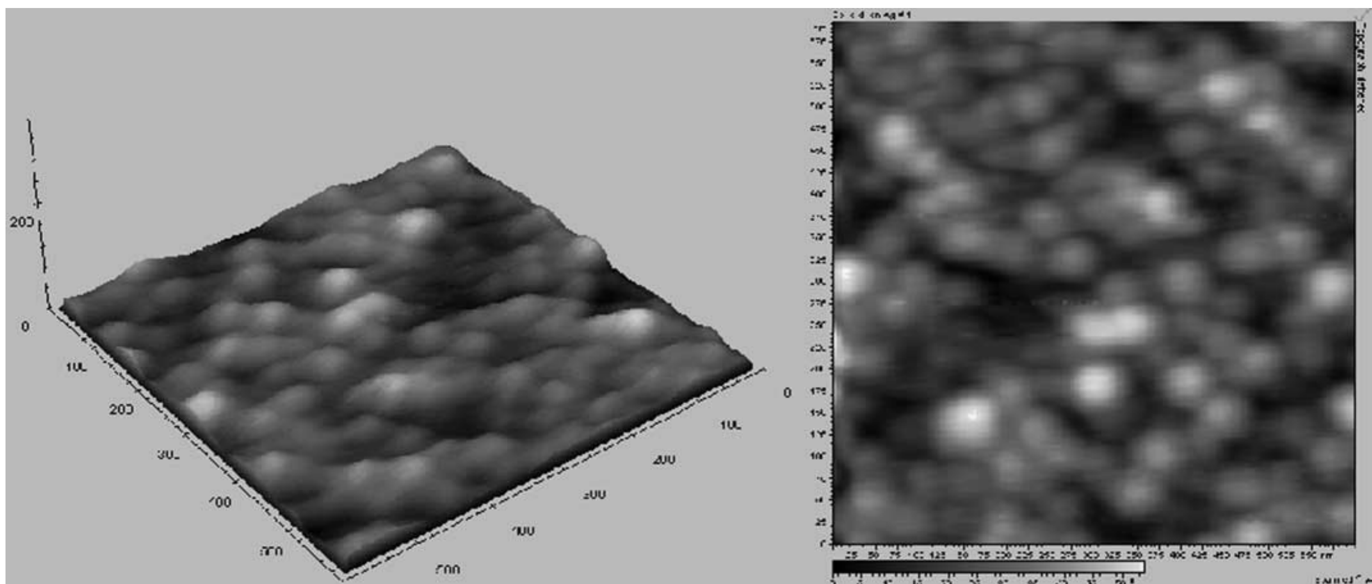

FIG. 2. AFM scan of silver surface deposited on top of PSL sphere.

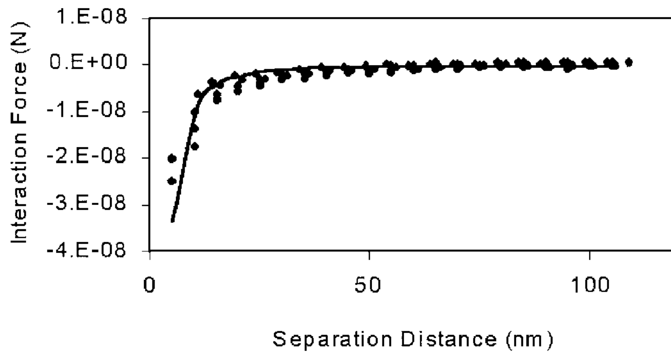

FIG. 3. The interaction of copper-coated PSL spheres with silicon dioxide as the spheres on the UHVAFM cantilever approach the silicon dioxide substrate. The data is fit by the Derjaguin approximation (Eq. [9]). Each data point is the average of 50 measurements (10 measurements on each of 5 spheres).

Any degree of deformation can be properly treated in the adhesion model based on the applied load and bulk modulus of each interacting material. In these cases, the Hamaker constant can be determined.

RESULTS AND DISCUSSION

Figure 3 compares UHVAFM measurements of the interaction forces between copper-coated PSL spheres and silicon dioxide substrates to predictions using the Derjaguin approximation for a sphere interacting with a flat plate (Eq. [9]). Each data point is the average obtained for 5 different sphere/cantilever systems when 10 measurements were made for each sphere. Similar measurements were made for all of the other systems studied, including copper, silver, and silicon dioxide interacting with copper, silver, silicon dioxide, titanium nitride, parylene-N, crosslinked parylene-N and PTFE. The histogram in Fig. 4 shows the use of the pull-off force model developed by Cooper *et al.* (6–9) to describe the pull-off force for the copper-coated PSL/silicon dioxide system from Fig. 3. In this case, measurements were made using five different copper-coated PSL spheres and a silicon dioxide substrate. The interaction force for each sphere was measured 10 times. Due to roughness on the substrate and coated spheres, a range of interaction forces was measured. Cooper's model accounts for the roughness effects and predicts a corresponding range of interaction forces.

FIG. 4. The predicted interaction force between copper-coated PSL spheres and silicon dioxide as the spheres on the UHVAFM cantilever are removed from the silicon dioxide substrate. The solid dark line is the average measured force, and the dotted lines represent ±1, 2, or 3 standard deviations from the average measurement.

TABLE 1
A Comparison of Values of A_{12} Measured in This Work, Calculated Using Approximate Methods, and Taken Directly from the Literature

System	Calculated Values using		Literature Values			Experimental			References
						Vacuum		Nitrogen	
	TWA	SS	low	avg	high	Contact	Noncontact	Contact	
Ag–Ag	20.30	48.78	16.40	34.20	50.00	38.20	39.10	37.90	33–41
Cu–Cu	24.82	40.21	28.40	33.00	40.00	27.30	27.60	27.10	33–41
SiO_2–SiO_2	6.55	6.96	8.55	21.23	50.00	—	—	7.20	33–41
PTFE–PTFE	3.63	5.54	5.05	5.56	6.02	—	—	—	39–41
TiN–TiN	15.73	18.23	—	—	—	—	—	—	—
Parylene-n–Parylene-n	11.10	7.09	—	—	—	—	—	—	—
Ag–Cu	22.45	44.28	21.58*	33.59*	42.24*	32.60	34.00	32.40	—
Ag–SiO_2	11.12	18.42	11.84*	26.59*	47.22*	12.92	13.40	12.70	—
Ag–PTFE	8.34	16.44	8.87*	13.55*	16.39*	13.70	12.60	13.60	—
Ag–Parylene-n	14.30	18.50	—	—	—	11.80	10.20	11.60	—
Ag–Cross linked Parylene-n	14.30	18.50	—	—	—	12.10	10.60	12.00	—
Ag–TiN	16.80	20.54	—	—	—	16.40	17.30	16.10	—
Cu–SiO_2	11.60	16.73	15.58*	26.47*	44.72*	14.10	14.20	13.90	—
Cu–PTFE	8.72	14.92	11.68*	13.31*	15.52*	13.10	11.20	12.80	—
Cu–Parylene-n	15.00	16.88	—	—	—	9.80	8.90	10.10	—
Cu–Cross linked Parylene-n	15.00	16.88	—	—	—	11.00	9.90	11.10	—
Cu–TiN	17.59	20.92	—	—	—	12.30	14.20	12.50	—
SiO_2–PTFE	4.87	6.17	6.41*	10.68*	17.35*	—	—	7.60	—
SiO_2–Parylene-n	8.55	6.86	—	—	—	—	—	6.80	—
SiO_2–Cross linked Parylene-n	8.55	6.86	—	—	—	—	—	6.90	—
SiO_2–TiN	10.10	12.04	—	—	—	—	—	8.80	—

Note. (*) Calculated from first four values of A_{1V1} with relationship $A_{1V2} = \sqrt{A_{1V1}A_{2V2}}$.

Comparisons between literature Hamaker constants, those calculated with approximate methods, and those found through our contact and noncontact measurements are shown in Table 1. Literature values for the materials studied here are only available for materials interacting with themselves through vacuum. Such interactions are represented by A_{1V1}, in which two surfaces of material "1" are interacting through a vacuum. Values for A_{1V1} for silver, copper, silicon dioxide, and PTFE were taken from the literature. Literature values of A_{1V3} presented in Table 1 in the column labeled "Literature Values" were calculated using the relation (13)

$$A_{1V3} = \sqrt{A_{1V1}A_{3V3}}. \quad [11]$$

Direct measurements were made for PTFE, parylene-N, and TiN in contact with other materials, but not for contact with themselves, A_{1V1} A_{1V1} was measured directly for all the other materials studied. Measured values of A_{1V1} for PTFE were determined by using Eq. [11] with measured constants for A_{3V3} (Ag = 3 in this case) and A_{1V3} (PTFE = 1 in this case). This value of A_{1V1} for PTFE was compared with literature values. Measured values of A_{1V1} for parylene-N and TiN were determined by using Eq. [11] with measured constants for A_{3V3} (Ag = 3 in this case) and A_{1V3} (parylene-N or titanium nitride = 1 in this case). These values of A_{1V1} for parylene-N and titanium nitride were not compared with literature values, as literature values could not be found for these materials.

The range of reported Hamaker constant values can be quite large, as is the case for the silicon dioxide systems. This indicates the need to measure the Hamaker constant for specific systems of interest, rather than select literature values that may not be representative. Since the range of Hamaker constants found in the literature is quite large for the systems of interest, the lowest and highest values and the average of all values were considered in comparison to the measured values reported here. All of the measured values fall within the range of reported values. However, since the literature range was so wide for some systems and values were unavailable for others, the Hamaker constants were also calculated using approximate methods for a second basis of comparison. The results of these calculations are shown in columns 2 and 3 of Table 1. As can be seen, there is some agreement between the predictions in columns 2 and 3 and the measured values for the polymer systems, but there is less agreement for the metal-dielectric systems. This may be due to the fact that optical properties for metal films can be affected by several material properties, such as grain size and the presence and thickness of surface oxides, that are not considered in the adhesion measurements (41). Therefore, literature optical constants used to calculate the Hamaker constants in Table 1

using approximate methods may not be representative of materials used in these experiments.

There is very little difference between the measured Hamaker constants in vacuum and in nitrogen. It is expected that the VDW forces should be greater in vacuum than in nitrogen, as the nitrogen shields the two interacting surfaces and pushes the system toward a condition where retarded, rather than nonretarded, Hamaker constants should be used. The negligible difference between the Hamaker constants obtained in UHV and in nitrogen suggests that the nonretarded approach may be correct, and that the presence of nitrogen is inconsequential when the two interacting surfaces are in close contact. This result also indicates that we have effectively removed adsorbed moisture from the interacting surfaces during the adhesion force measurements in nitrogen. In UHV, the adsorbed moisture on the interacting surfaces is likely to be negligible. There are several possible limitations in the calculations of the adhesion model that may account for the difference between contact and noncontact Hamaker constants. These include effects of asperity deformation and asperity shape, the number of experimental adhesion force measurements made in each system, and the convolution of partial cohesive failure of a material with VDW forces during the pull-off method of adhesion measurement.

Table 2 shows the average measured Hamaker constant and the percent difference between the contact and noncontact methods for all the systems in Table 1. In Table 2, it is clear that the best agreement between Hamaker constants measured in and out of contact was achieved for the metal/metal or metal/silicon dioxide systems. Conversely, the polymer (PTFE, parylene, and cross-linked parylene) systems had the largest degree of variance among Hamaker constants measured by the two methods.

The size and shape of the asperities may affect the adhesion model predictions. The model developed previously by Cooper

TABLE 2

Comparison of Experimental AFM Measurements of A_{12}, Determined with the Derjaguin Approximation and with the Contact Adhesion Model

System	Vacuum		Percent difference
	Contact	Noncontact	
Ag–Ag	38.20	39.10	2.30
Cu–Cu	27.30	27.60	1.09
Ag–Cu	32.60	34.00	4.12
Ag–SiO_2	12.92	13.40	3.58
Ag–PTFE	13.70	12.60	8.73
Ag–Parylene-n	11.80	10.20	15.69
Ag–Crosslinked Parylene-n	12.10	10.60	14.15
Ag–TiN	16.40	17.30	5.20
Cu–SiO_2	14.10	14.20	0.70
Cu–PTFE	13.10	11.20	16.96
Cu–Parylene-n	9.80	8.90	10.11
Cu–Crosslinked Parylene-n	11.00	9.90	11.11
Cu–TiN	12.30	14.20	13.38

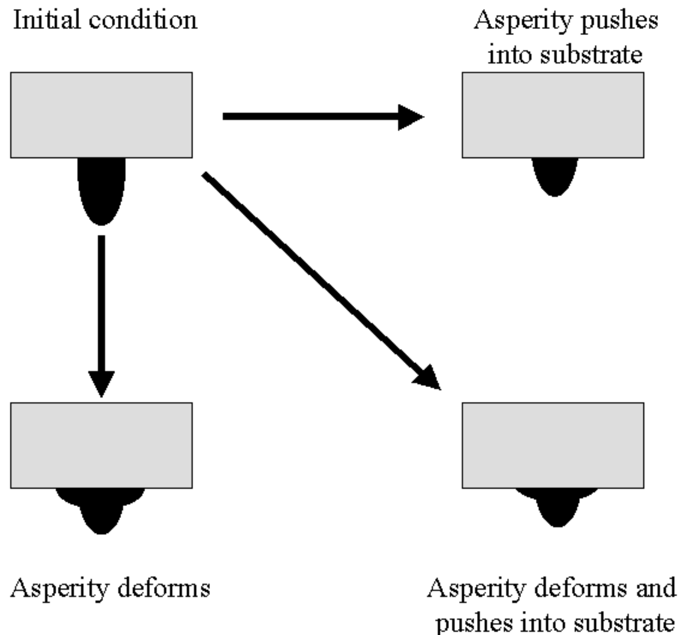

FIG. 5. Schematic description of asperity deformation.

et al. was validated for a PSL/water/silicon dioxide system and also for alumina particles interacting with silicon dioxide and copper substrates in water and air. In these systems, it was assumed that asperities on the two surfaces were hemispherical, and that the asperities deformed by averaging two types of deformation. The first type of deformation involves pushing the asperity back into the material without changing the shape of the asperity. The second type of deformation involves pushing the asperity to make it deform outward, with no deformation of the substrate. The current model assumes that each type of deformation occurs, and that the total deformation is influenced equally by each of these two types. In other words, we assume that the asperity is pushed into the substrate and that the asperity deforms significantly. Figure 5 presents a schematic illustration of the assumed deformation. Although these assumptions account sufficiently for asperity deformation in the model systems studied previously, the deformation of asperities is complex, and an inaccurate description of the deformation of these structures can influence the calculated adhesion (31). Asperities on the polymer substrates are larger than those on the PSL spheres used to validate the original model. Improperly accounting for the complex problem of asperity deformation in larger asperities may lead to a larger error. If only one type of deformation is assumed in the simulations, either the asperity does not deform but pushes into substrate or the asperity deforms and does not push into substrate. To determine the effect of the assumed deformation on the predicted Hamaker constants, the constants were calculated for each system assuming that all of the deformation occurred on the asperity or that all of the deformation occurred on the substrate. With these approaches, the Hamaker constants found for each deformation case (substrate only, asperity

only) bound the constant found from the noncontact force curve for all cases shown here. This indicates that within our ability to account for asperity deformation, the Hamaker constant values found through contact and noncontact measurements are the same. In addition to asperity size, the shape of asperities may also affect the results. The asperities in the pull-off force model were modeled as hemispheres. However, if an asperity has a nonuniform shape, the volume of interaction estimated by modeling asperities as hemispheres and distributing these hemispheres on the substrates to match the measured fractional coverage of each substrate may not describe the true interaction volume between the asperity and the opposing surface. A change of 10% in fractional coverage by asperities causes the Hamaker constant for the system to change by approximately 15 to 20%.

The limited number of measurements made relative to the number of model simulations performed to extract the Hamaker constants may also give an inaccurate estimate of these constants. When the model is used to simulate interactions between two surfaces, 10,000 simulations are performed to obtain an average predicted adhesion force. The standard deviation in this adhesion force can typically be quite large depending on the roughness characteristics of the interacting surfaces. Due to limitations on resources, only a limited number of measurements were made, with typically five cantilevers used 50 times each for each interaction measurement. Further, while a single cantilever can be used for more than one measurement, measurements made after the first interaction can be contaminated if material from the substrate pulls off the substrate and adheres to the sphere. This contamination can occur in metals interacting with other metals and oxides (44), and it may also occur with polymers that may fail cohesively. The cohesive failure of a polymer during AFM measurement was observed when PSL spheres interacting with silicon dioxide were seen to increase in roughness with the number of interactions until a steady roughness was reached (6, 7). In this case, rather than measuring the adhesive interaction strength, we may have measured a combination of the adhesive and cohesive strengths. Also, a sphere that fails cohesively can only be used in a limited number of interaction force measurements, and the average adhesion force of the resulting small sampling may be different than that found when the number of interactions sampled is on the order of that used in the model.

In general, the cohesive failure of one of the materials causes a convolution of VDW forces with other interactions. When the sample on the cantilever interacts strongly enough with the surface to cause partial cohesive failure of one of the materials, the removal force measured includes other forces such as the energy required to stretch polymeric molecules or to break chemical bonds. In the systems studied here, if cohesive failure occurred it was small enough that it did not greatly affect the measurements made, as evidenced by the good agreement between the pull-off (contact) and noncontact approaches for measuring the adhesion.

CONCLUSIONS

Hamaker constants were measured for metal, dielectric, and barrier materials of interest during IC interconnect processing. The measurements were made using an AFM in nitrogen and vacuum environments. A new method of determining the Hamaker constant was examined using an adhesion model developed previously. The values determined by this model compared well with those found in the literature and those calculated with spectral data found in the literature. The difference between the Hamaker constants determined using both contact and noncontact AFM measurements was very small. The variations indicate that the model may not accurately account for morphological or mechanical properties for some systems. In particular, it is likely that the shape and deformation of asperities need to be more accurately described to improve the agreement between model predictions and experimental measurement. It also was shown that with proper care the effect of adsorbed water can be eliminated from VDW force measurements using an AFM. The contact measurement approach showed good agreement with the noncontact method when the roughness, geometry, and physical properties of the two surfaces were appropriately described. This demonstrates that a contact measurement can provide an accurate description of adhesion in contact and also a good estimate of the Hamaker constant in the systems studied here.

ACKNOWLEDGMENTS

The authors are grateful to the National Science Foundation/Semiconductor Research Corporation Engineering Research Center for Environmentally-Benign Semiconductor Manufacturing (EEC-9528813) for both financial support and technical guidance on this project. The authors thank Molecular Imaging Corp. for assistance with the AFM. The authors are also grateful to the Center for Interactive Nano-Visualization in Science and Engineering Education, the Center for Solid State Electronics Research, and the Center for Solid State Science at Arizona State University. The authors also thank Michael Kozicki at Arizona State University for assistance with the UHVAFM measurements. The authors are grateful to the National Science Foundation (CAREER: CTS 9984620) for financial support.

REFERENCES

1. Zeng, Y., Ph.D. dissertation, Arizona State University, 1999.
2. Muraka, S. P., and Hymes, S. W., *Crit. Rev. Solid State Mater. Sci.* **20**(2), 87 (1995).
3. Dabral, S., Zhang, X., Wang, B., Yang, G.-R., Lu, T.-M., and McDonald, J. F., *Mater. Res. Soc. Symp. Proc.* **381,** 205 (1995).
4. Beach, W. F., Lee, C., Basset, D. R., Austin, T. M., and Olson, R., Xylylene polymers, *in* "Encyclopedia of Polymer Science and Engineering," 2nd ed., Vol. 17, pp. 990–1023, Wiley, New York, 1989.
5. Gleason, K., Kwan, M. C., and Lewis, H. P., *Abstr. Pap. Am. Chem. Soc.* **219,** 111 (2000).
6. Cooper, K., Ohler, N., Gupta, A., and Beaudoin, S., *J. Colloid Interface Sci.* **222,** 63 (2000), doi:10.1006/jcis.1999.6561.
7. Cooper, K., Gupta, A., and Beaudoin, S., *J. Colloid Interface Sci.* **228,** 213 (2000), doi:10.1006/jcis.2000.6881.
8. Cooper, K., Gupta, A., and Beaudoin, S., *J. Colloid Interface Sci.* **234,** 284 (2001), doi:10.1006/jcis.2000.7276.

9. Cooper, K., Gupta, A., and Beaudoin, S., *J. Electrochem. Soc.*, in press (2001).
10. Sounilhac, S., Barthel, E., and Creuzet, F., *J. Appl. Phys.* **85**(1), 222 (1999).
11. Sounilhac, S., Barthel, E., and Creuzet, F., *Appl. Surf. Sci.* **140,** 411 (1999).
12. Gady, B., Schleef, D., Reifenberger, R., Rimai, D., and DeMejo, L. P., *Phys. Rev. B.* **53**(12), 8065 (1996).
13. Israelachvili, J., "Intermolecular and Surface Forces," 2nd ed., Academic Press, San Diego, 1992.
14. Evans, D. F., and Wennerstrom, H., "The Colloidal Domain," VCH, London, 1994.
15. Lifshitz, E. M., *Sov. Phys. JETP* **2,** 73 (1956).
16. Dzyaloshinskii, I. E., Lifshitz, E. M., and Pitaevskii, L. P., *Adv. Phys.* **10,** 165 (1961).
17. Ninham, B. W., and Parsegian, V. A., *Biophys. J.* **10,** 646 (1970).
18. Hough, D. B., and White, L. R., *Adv. Colloid Interface Sci.* **14,** 3 (1980).
19. Ninham, B. W., and Parsegian, V. A., *J. Chem. Phys.* **52**(9), 4578 (1970).
20. Mahanty, J., and Ninham, B. W., "Dispersion Forces," Academic Press, New York, 1976.
21. Tabor, D., F. R. S., and Winterton, R. H. S., *Proc. Roy. Soc. A.* **312,** 435 (1969).
22. Ackler, H. D., French, R. H., and Chiang, Y. M., *J. Colloid Interface Sci.* **179,** 460 (1996), doi:10.1006/jcis.1996.0238.
23. French, R. H., *J. Am. Ceram. Soc.* **83**(9), 2117 (2000).
24. Bergstrom, L., *Adv. Colloid Interface Sci.* **70,** 125 (1997).
25. Ducker, W. A., and Senden, T. J., *Langmuir* **8,** 1831 (1992).
26. Chechenin, N. G., Bottinger, J., and Krog, J. P., *Thin Solid Films* **304,** 70 (1997).
27. Cleveland, J. P., Manne, S., Bocek, D., and Hansma, P. K., *R. Sci. Instrum.* **64**(2), 403 (1993).
28. Thundat, T., Zheng, X. Y., Chen, G. Y., and Warmack, R. J., *Surf. Sci. Lett.* **294,** L939 (1993).
29. Torii, A., Saski, M., Hane, K., and Okuma, S., *Sens. Actuators A.* **40,** 71 (1994).
30. Sugawara, Y., Ohta, M., Konishi, T., and Morita, S., *Wear* **168,** 13 (1993).
31. Biggs, S., and Spinks, G. J., *J. Adhes. Sci. Technol.* **12,** 461 (1998).
32. Drummond, C. J., Georgaklis, G., and Chan, D. Y. C. *Langmuir* **12**(11), 2617 (1996).
33. Visser, J., *Adv. Colloid Interface Sci.* **3,** 331 (1972).
34. French, R. H., Cannon, R. M., DeNoyer, L. K., and Chiang, Y. M., *Solid State Ionics* **75,** 13 (1995).
35. Parsegian, V. A., and Weiss, G. H., *J. Colloid Interface Sci.* **81**(1), 285 (1981).
36. Busnaina, A., Taylor, J., and Kashkoush, I., *J. Adhes. Sci. Technol.* **7**(5), 441 (1993).
37. Middleman, S., and Hochberg, A. K., "Process Engineering Analysis in Semiconductor Device Fabrication," McGraw–Hill, New York, 1993.
38. Moses, A. J., "Handbook of Electronic Materials," Vol. 1, Optical Materials Properties, Plenum, New York, 1971.
39. Palik, E. D., "Handbook of Optical Constants," Academic Press, New York, 1985.
40. Palik, E. D., "Handbook of Optical Constants II," Academic Press, New York, 1991.
41. Palik, E. D., "Handbook of Optical Constants III," Academic Press, New York, 1998.
42. Hummel, D. O., "Atlas of Polymer and Plastic Analysis," Scholl, New York, 1978.
43. Landman, U., Luedtke, W. D., Burnham, N. A., and Colton, R. J., *Science* **248,** 454 (1990).